AAS 25-207

ORBITING SPACECRAFT RELATIVE MOTION IN THE INERTIAL FRAME FOR INERTIALLY FIXED CONSTRAINTS

Julian Hammerl* **and Hanspeter Schaub†**

While the description of orbiting spacecraft relative motion is usually done in the rotating Hill frame due to analytical first-order solutions and the intuitive shape of the relative orbits, it is disadvantageous for mission design requirements that are fixed in the inertial frame. This includes distributed space telescopes aligned with inertial targets as well as formations and servicing operations with inertially fixed keep-in/out zones, e.g. constraints imposed by the Sun direction. This paper studies the analytical first-order inertial frame solutions of the relative motion of orbiting spacecraft and derives geometrically meaningful invariants of motion for inertial frame relative orbits. Scenarios with both bounded and secularly drifting relative motion are investigated. Solutions are presented for both circular and elliptic chief motions and the new invariants of the relative motion are compared to relative orbit elements and differential classic orbit elements.

INTRODUCTION

The relative motion of an orbiting deputy spacecraft with respect to a chief spacecraft is most commonly described in a rotating frame aligned with the radial position vector of the chief, often referred to as the Hill frame[1] or the Local-Vertical-Local-Horizontal (LVLH) frame. Some of the benefits of the description in the Hill frame are the existence of simple analytical solutions for circular orbits, such as for the Clohessy–Wiltshire equations,[2] the resulting intuitive shape of the relative orbits, and the fact that the out-of-plane motion is uncoupled from the in-plane motion. For bounded motion (no drift motion), the relative orbit has the shape of an ellipse (or in simpler cases a single point) in the orbital plane and is either centered at the chief or offset in the along-track direction. A difference in the semi-major axis of the two spacecraft results in drift motion in the along-track direction. In the most complex case for drift motion, the relative orbit is a spiral motion about the along-track direction.

However, the description in the Hill frame is disadvantageous for some mission design requirements. Distributed space telescopes have been proposed for large-aperture telescope architectures that cannot be realized with a single spacecraft.[3,4] Instead of having one spacecraft with all telescope components, a two-spacecraft formation consisting of one spacecraft equipped with the lens and another spacecraft equipped with the sensor is used. The VIrtual Super Optics Reconfigurable Swarm (VISORS) mission is a demonstration for such a concept.[5] Because a space telescope is

*Graduate Research Assistant, Ann and H.J. Smead Department of Aerospace Engineering Sciences, University of Colorado Boulder, Colorado Center for Astrodynamics Research, Boulder, CO, 80303 USA. AAS Member, AIAA Member julian.hammerl@colorado.edu

†Distinguished Professor and Department Chair, Schaden Leadership Chair, Ann and H.J. Smead Department of Aerospace Engineering Sciences, University of Colorado Boulder, Colorado Center for Astrodynamics Research, Boulder, CO, 80303 USA. AAS Fellow, AIAA Fellow

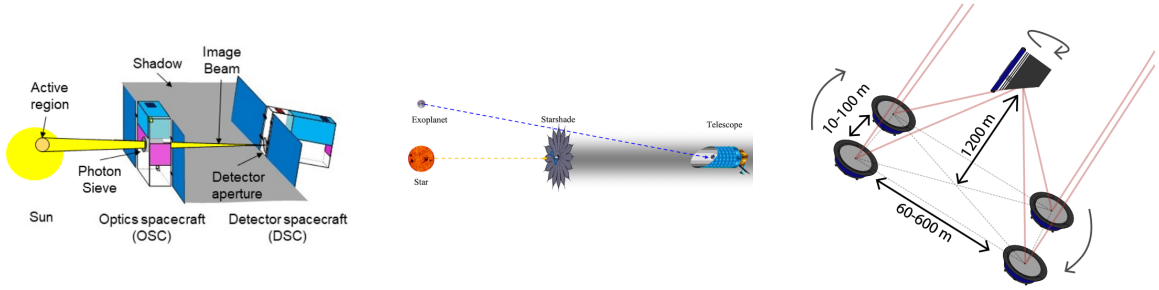

(a) VISORS (b) New Worlds Observer (c) LIFE mission

Figure 1: Concept figures of space missions with inertial constraints

commonly aligned with inertial targets, the description of relative motion is beneficial in the inertial frame, despite inertial frame relative orbits being more complex. That is, instead of expressing the relative position and velocity vectors of the deputy with respect to the chief in a rotating frame, it may be beneficial to describe these vectors in inertial frame components. Missions such as New World Observer,[6] where a giant starshade[7] is used to block the light from a star while searching for exoplanets, may also benefit from a description in the inertial frame. Other missions such as the Terrestrial Planet Finder[8] (TPF, canceled in 2011) and Large Interferometer For Exoplanets[9] (LIFE, in development) proposed to use a nulling interferometer consisting of multiple spacecraft to search for exoplanets. These exoplanet search missions were planned to be located around the Sun-Earth L2 Lagrange point. Thus, the relative motion occurs far away from a planet,[10,11] in contrast to the relative motion of two spacecraft orbiting a planet at lower altitudes as explored in this current work. Other mission concepts call for formations where the spacecraft never eclipse each other, or where one spacecraft is desired to be in the shadow of the other for prolonged periods. For example, the Project for On-Board Autonomy 3 (PROBA-3) mission is a formation flying demonstration mission that launched in December 2024, consisting of an occulter spacecraft that casts the Sun's shadow on a coronagraph spacecraft to study the Sun's faint corona. For spacecraft orbiting Earth, this imposes a keep-out or keep-in zone that is fixed in a quasi-inertial frame (because the Sun direction changes slowly).

In a similar fashion, such inertially fixed keep-out or keep-in zones may be introduced for spacecraft servicing and docking operations. For example, during rendezvous it may be beneficial to maintain certain lighting conditions, or to keep line-of-sight with another inertially fixed target. Relative motion constraints for docking operations are often described in the body frame of the target spacecraft. If the target satellite is not rotating, the body frame of the target remains aligned with the inertial frame, and the insights from the inertial frame relative motion can be applied to the body frame. Finally, plasma wakes also motivate a relative motion description in the inertial frame. Plasma wakes form in the anti-ram-side direction behind the spacecraft if the ion thermal velocity is greater than the electron thermal velocity,[12] where the ram-side is determined by the spacecraft velocity relative to the bulk velocity of the ions. The plasma and spacecraft charging dynamics are more complex inside this wake, and inter-spacecraft electrostatic forces may also be stronger.[13] This motivates to stay inside the wake to study the plasma and spacecraft charging dynamics, or outside to minimize electrostatic perturbations.[14] In Low Earth Orbit (LEO), the ion bulk velocity is negligibly small, so the wake is approximately fixed in the spacecraft velocity frame.[15] Outside Earth's magnetosphere, in contrast, the ions move with the solar wind. If the spacecraft velocity is

negligibly small compared to the solar wind velocity, the wake forms in the anti-sun direction and is quasi-inertially fixed.[16]

The aforementioned mission scenarios benefit from a relative motion description in the inertial frame. A large body of work exists in the literature about relative motion described in the Hill frame,[17] for linear and non-linear models as well as near-circular and eccentric reference orbits. Constraints such as keep-in and keep-out zones are also usually described in the Hill frame or body frame of the target. Hill frame fixed keep-out zones are convenient for situations with larger spacecraft separation distances such as safety ellipses during approach of a spacecraft to the International Space Station.[18] Body frame fixed keep-out zones are often used for docking operations.[19] Some work exists for relative motion in the spacecraft velocity frame.[20] This description is especially advantageous for atmospheric entry trajectories of two spacecraft or highly eccentric chief orbits. Inertially constrained relative motion around a planet has only been studied for a very specific orbit to maximize the average power generation,[21,22] but keep-out zones or general orbits were not investigated.

This paper researches analytical first-order solutions to the orbiting spacecraft relative motion as seen by the inertial frame. The relative equations of motion (EOM) are derived by transforming the Hill frame first-order EOM into the inertial frame. First, this is done using the closed-form solution of the Clohessy-Wiltshire relative motion equations for circular chief orbits. To make the inertial relative motion more intuitive, the chief orbital elements and the six parameters that define the Clohessy-Wiltshire closed-form solution are related to the shape, size and orientation of the relative orbit in the inertial frame. That is, novel geometrically meaningful relative motion invariants are derived for the inertial relative orbits. This allows for an easier analysis of violations of keep-in and keep-out zones that are fixed in the inertial frame. Next, the study is extended to elliptic chief orbits, using the non-dimensional orbit element difference description of relative motion.

BACKGROUND

Two spacecraft are orbiting a central body in close proximity to each other. Given the inertial position of the chief (target spacecraft) $\boldsymbol{r}_c$ and the deputy (servicing spacecraft) $\boldsymbol{r}_d$, the relative position vector is defined as

$$\boldsymbol{\rho} = \boldsymbol{r}_d - \boldsymbol{r}_c \tag{1}$$

Relevant Coordinate Frames

The relative motion is commonly described in a rotating frame $\mathcal{H} : \{\hat{\boldsymbol{h}}_r, \hat{\boldsymbol{h}}_\theta, \hat{\boldsymbol{h}}_h\}$ centered at the chief C with axes

$$\hat{\boldsymbol{h}}_r = \frac{\boldsymbol{r}_c}{|\boldsymbol{r}_c|} \tag{2a}$$

$$\hat{\boldsymbol{h}}_\theta = \hat{\boldsymbol{h}}_h \times \hat{\boldsymbol{h}}_r \tag{2b}$$

$$\hat{\boldsymbol{h}}_h = \frac{\boldsymbol{r}_c \times \dot{\boldsymbol{r}}_c}{|\boldsymbol{r}_c \times \dot{\boldsymbol{r}}_c|} \tag{2c}$$

where $\dot{\boldsymbol{r}}_c$ is the inertial velocity of the chief. This frame is referred to as the Hill frame[1] and is similar to the Local-Vertical-Local-Horizon (LVLH) frame $\mathcal{L} : \{\hat{\boldsymbol{l}}_1 = \hat{\boldsymbol{h}}_\theta,\ \hat{\boldsymbol{l}}_2 = -\hat{\boldsymbol{h}}_h,\ \hat{\boldsymbol{l}}_3 = -\hat{\boldsymbol{h}}_r\}$. The first axis of the Hill frame is aligned with the orbit radial direction of the chief and the third axis is aligned with the orbit normal direction. Another frame $\mathcal{N} : \{\hat{\boldsymbol{n}}_1, \hat{\boldsymbol{n}}_2, \hat{\boldsymbol{n}}_3\}$ is used with inertially fixed directions of the frame axes $\hat{\boldsymbol{n}}_1, \hat{\boldsymbol{n}}_2, \hat{\boldsymbol{n}}_3$. Figure 2 illustrates the Hill frame and Inertial frame.

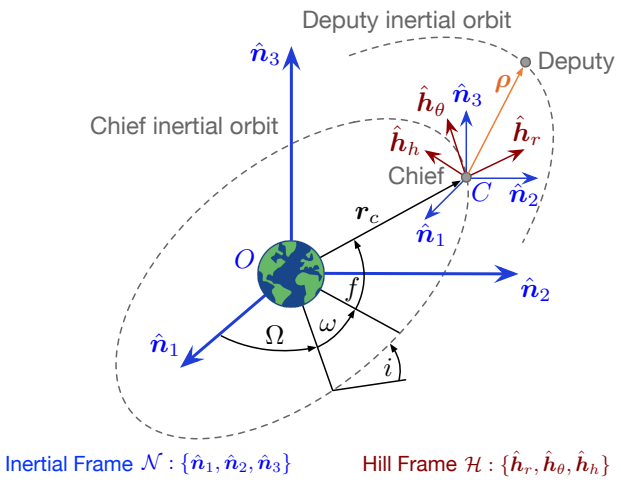

Figure 2: Illustration of Hill frame and Inertial frame: The Hill frame $\mathcal{H}$ is centered at the chief and rotates as the chief orbits the central body, with $\hat{\boldsymbol{h}}_r$ aligned with the orbit radial direction of the chief and $\hat{\boldsymbol{h}}_h$ aligned with the orbit normal direction. The inertial frame $\mathcal{N}_O$ is located at the central body with fixed directions of the frame axes. A moving frame $\mathcal{N}_C$ is used that is centered at the chief, but its axes remain aligned with the inertial frame.

The direction cosine matrix (DCM) $[HN]$ to map from the inertial frame $\mathcal{N}$ to the Hill frame $\mathcal{H}$ may be obtained using the chief orbit elements. Using the DCMs for a generic rotation θ about the first frame axis

$$[M_1(\theta)] = \begin{bmatrix} 1 & 0 & 0 \\ 0 & \cos\theta & \sin\theta \\ 0 & -\sin\theta & \cos\theta \end{bmatrix} \tag{3}$$

and the generic DCM about the third frame axis

$$[M_3(\theta)] = \begin{bmatrix} \cos\theta & \sin\theta & 0 \\ -\sin\theta & \cos\theta & 0 \\ 0 & 0 & 1 \end{bmatrix} \tag{4}$$

the DCM for a (3-1-3) Euler angle rotation (Ω, i, ω) is written as[23]

$$[PN(\Omega, i, \omega)] = [M_3(\omega)][M_1(i)][M_3(\Omega)] \tag{5}$$

where Ω is the right ascension of the ascending node (RAAN), i is the orbit inclination, and ω is the argument of periapsis. The frame $\mathcal{P} : \{\hat{\boldsymbol{p}}_1, \hat{\boldsymbol{p}}_2, \hat{\boldsymbol{p}}_3\}$ is the perifocal frame, in which the first axis points from the focus of the orbit (the central body) to periapsis, the third axis points in the chief orbit angular momentum direction, and the second axis completes the right-handed coordinate frame. To map from the perifocal frame $\mathcal{P}$ to the Hill frame $\mathcal{H}$, another rotation around the third frame axis is performed using the true anomaly f

$$[HP(f)] = [M_3(f)] \tag{6}$$

Thus, the DCM to map from the inertial frame to the Hill frame is equal to

$$[HN(\Omega, i, \omega, f)] = [HP][PN] = [M_3(f)][M_3(\omega)][M_1(i)][M_3(\Omega)] \tag{7}$$

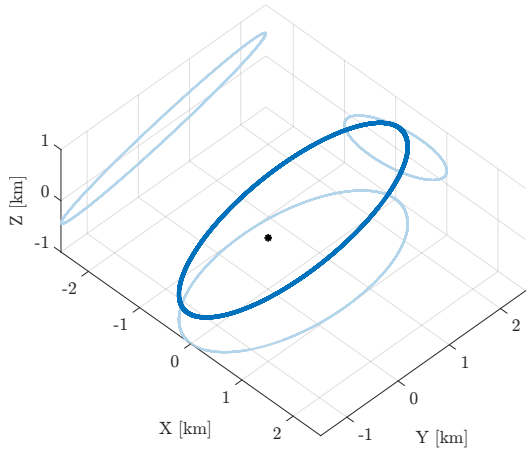

(a) Motion 1: $A_0 = 1,\ \alpha = -60$ deg, $x_{\text{off}} = 0,\ y_{\text{off}} = 0.5,\ B_0 = 0.5,\ \beta = 0$

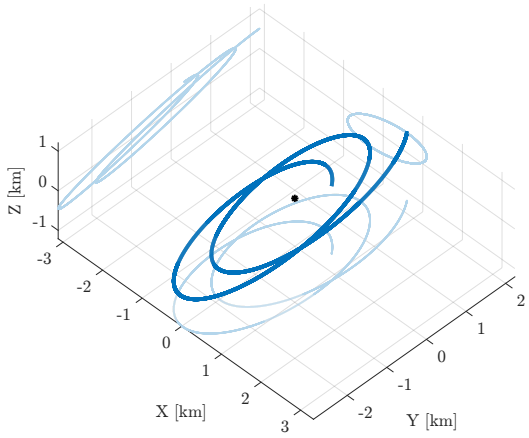

(b) Motion 2: $A_0 = 1,\ \alpha = -60$ deg, $x_{\text{off}} = 0.1,\ y_{\text{off}} = 0.5,\ B_0 = 0.5,\ \beta = 0$

Figure 3: Relative motion in Hill frame for a circular chief orbit: A_0 creates a 2-by-1 relative orbit ellipse that is offset in the y-direction by y_{off}. Drift motion is induced by x_{off}. The projections of the relative orbit on the three planes are shown in lighter color.

Cartesian Coordinate Description

The relative position vector $\boldsymbol{\rho}$ of the deputy relative to the chief in Hill-frame components is

$$^{\mathcal{H}}\boldsymbol{\rho} = \begin{bmatrix} x \\ y \\ z \end{bmatrix} \tag{8}$$

where the left superscript indicates that the vector is expressed in Hill frame $\mathcal{H}$ components, and x, y, z are the relative position coordinates in the Hill frame. In this frame, x and y describe the relative motion in the chief orbit plane while z describes any out-of-plane motion. Assuming a circular chief orbit (eccentricity $e = 0$) and small separation distances between the two spacecraft ($|\boldsymbol{\rho}| \ll |\boldsymbol{r}_c|$), the relative equations of motion (EOM) in the Hill frame are equal to[1]

$$\ddot{x} - 2n\dot{y} - 3n^2 x = 0 \tag{9a}$$

$$\ddot{y} + 2n\dot{x} = 0 \tag{9b}$$

$$\ddot{z} + n^2 z = 0 \tag{9c}$$

These relative EOM are known as the Clohessy-Wiltshire (CW) equations. Using the semi-major axis a of the chief orbit and the standard gravitational parameter μ of the central body, the mean motion n is determined by $n = \sqrt{\mu/a^3}$. The analytical solution to the CW equations is equal to[2,3]

$$x(t) = A_0 \cos(nt + \alpha) + x_{\text{off}} \tag{10a}$$

$$y(t) = -2A_0 \sin(nt + \alpha) - \frac{3}{2} nt x_{\text{off}} + y_{\text{off}} \tag{10b}$$

$$z(t) = B_0 \cos(nt + \beta) \tag{10c}$$

The six relative motion parameters in Eq. (10) are called the linearized relative orbit elements (LROEs) and are the invariants of the linearized relative motion:

- In-plane sinusoidal amplitude A_0
- In-plane phase angle α
- Orbit-radial offset x_{off}
- Along-track offset at epoch y_{off}
- Out-of-plane sinusoidal amplitude B_0
- Out-of-plane phase angle β

These geometrically insightful invariants of motion are determined through the initial conditions and fully define the relative motion under the given assumptions.

Examining Eq. (10), one finds that the in-plane motion corresponds to a 2-by-1 ellipse in which the along-track amplitude is twice the orbit-radial amplitude, and the out-of-plane motion corresponds to an unforced oscillator. The motion may be offset in the y-direction with y_{off} or the x-direction with x_{off}. An offset x_{off} causes a drift in the along-track direction y over time due to the difference in semi-major axis of the two spacecraft. Thus, x_{off} must be zero for bounded motion. For a simple lead-follower formation, all relative motion parameters besides y_{off} are zero. Some relative orbit shapes in the Hill frame are shown in Fig. 3.

Orbit Element Difference Description

Given the general orbit elements

$$\boldsymbol{oe} = [a, e, i, \Omega, \omega, M_0]^T \tag{11}$$

with semi-major axis a, eccentricity e, inclination i, right ascension of the ascending node Ω, argument of periapsis ω and initial mean anomaly M_0, the orbit element differences between the deputy and the chief spacecraft are equal to[23]

$$\delta\boldsymbol{oe} = \boldsymbol{oe}_d - \boldsymbol{oe}_c = [\delta a, \delta e, \delta i, \delta\Omega, \delta\omega, \delta M_0]^T \tag{12}$$

This differential orbit elements (DOEs) description does not make any assumptions the eccentricity of the orbits. A semi-major axis difference δa between the two spacecraft causes the mean anomaly difference δM to drift over time. The relation between the differences in mean anomaly at time t and time t_0 is equal to

$$\delta M = \delta M_0 - \frac{3}{2}\frac{\delta a}{a}(M - M_0) \tag{13}$$

where M and M_0 are the mean anomalies of the chief at time t and time t_0, respectively. Assuming small relative orbit sizes, the relative position coordinates x, y, z can be expressed in terms of the orbit element differences and as a function of the chief true anomaly f for general orbit eccentricities

$$x(f) = \frac{r}{a}\delta a + \frac{ae\sin f}{\eta}\delta M - a\cos f\delta e \tag{14a}$$

$$y(f) = \frac{r}{\eta^3}(1 + e\cos f)^2\delta M + r\delta\omega + \frac{r\sin f}{\eta^2}(2 + e\cos f)\delta e + r\cos i\delta\Omega \tag{14b}$$

$$z(f) = r(\sin\theta\delta i - \cos\theta\sin i\delta\Omega) \tag{14c}$$

with the relation $\eta = \sqrt{1 - e^2}$, the true latitude $\theta = \omega + f$ and the chief orbit radius

$$r = \frac{p}{1 + e\cos f} = \frac{a(1 - e^2)}{1 + e\cos f} = \frac{a\eta^2}{1 + e\cos f} \tag{15}$$

Note that most terms in Eq. (14) include the orbit radius r, which varies with true anomaly f.

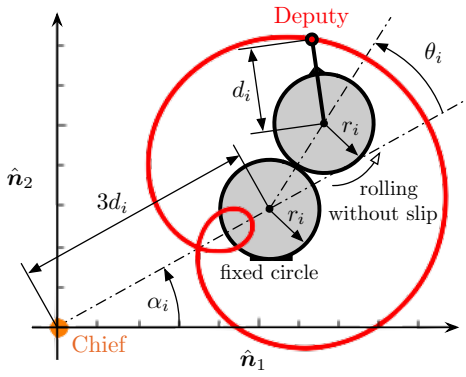

Figure 4: Inertial frame relative orbit elements: The relative motion in the inertial frame traces an epitrochoid curve, in which a circle with radius r_i rolls without slip on a fixed circle with radius r_i, and the curve is generated by a point that is at a distance of d_i away from the center of the rolling circle. The formation is $3d_i$ away from the origin and rotated by α_i.

CIRCULAR CHIEF ORBITS

First, the inertial relative motion is investigated for circular chief orbits using the Clohessy-Wiltshire equations. To express the relative motion in the inertial frame, the relative position $\boldsymbol{\rho}$ is simply mapped from the Hill frame $\mathcal{H}$ to the inertial frame $\mathcal{N}$ with the DCM $[NH] = [HN]^T$:

$$^{\mathcal{N}}\boldsymbol{\rho} = [NH] \cdot {}^{\mathcal{H}}\boldsymbol{\rho} = [HN]^T \cdot {}^{\mathcal{H}}\boldsymbol{\rho} = \begin{bmatrix} X \\ Y \\ Z \end{bmatrix} \tag{16}$$

For general chief orbit elements (Ω, i, ω) and relative orbit parameters, this results in a rather complex analytical expression that is difficult to analyze. Thus, to begin, it assumed that $\Omega = i = \omega = 0$. This corresponds to a description in the perifocal frame $\mathcal{P}$:

$$^{\mathcal{P}}\boldsymbol{\rho} = [HN(0,0,0,f)]^T \cdot {}^{\mathcal{H}}\boldsymbol{\rho} = [HP]^T \cdot {}^{\mathcal{H}}\boldsymbol{\rho} = \begin{bmatrix} X_p \\ Y_p \\ Z_p \end{bmatrix} \tag{17}$$

Once the relative motion is understood in the perifocal frame, it is rather straightforward to consider general chief orbit orientations. For a circular orbit, $f = nt$, so using Eqs. (10) and (17) as well as significant simplification results in the analytical expression

$$\begin{bmatrix} X_p(t) \\ Y_p(t) \\ Z_p(t) \end{bmatrix} = \begin{bmatrix} \frac{1}{2}\left(3A_0\cos\alpha - A_0\cos(\alpha+2nt) + 3ntx_{\text{off}}\sin(nt) + 2x_{\text{off}}\cos(nt) - 2y_{\text{off}}\sin(nt)\right) \\ \frac{1}{2}\left(-3A_0\sin\alpha - A_0\sin(\alpha+2nt) - 3ntx_{\text{off}}\cos(nt) + 2x_{\text{off}}\sin(nt) + 2y_{\text{off}}\cos(nt)\right) \\ B_0\cos(\beta+nt) \end{bmatrix} \tag{18}$$

Using the identities

$$A\sin t + B\cos t = \sqrt{A^2+B^2}\cos\left(t - \tan^{-1}\left(\frac{A}{B}\right)\right) \tag{19a}$$

$$A\sin t + B\cos t = -\sqrt{A^2+B^2}\sin\left(t - \tan^{-1}\left(\frac{B}{-A}\right)\right) \tag{19b}$$

and other well-known trigonometric identities, Eq. (18) is rewritten to significantly reduce its complexity

$$\begin{bmatrix} X_p(t) \\ Y_p(t) \\ Z_p(t) \end{bmatrix} = \begin{bmatrix} 3d_i \cos\alpha_i - d_i \cos(2nt - \alpha_i) - 2r_i \sin(nt - \phi_i) \\ 3d_i \sin\alpha_i - d_i \sin(2nt - \alpha_i) + 2r_i \cos(nt - \phi_i) \\ B_i \cos(nt - \beta_i) \end{bmatrix} \tag{20}$$

with

$$r_i = \frac{1}{2}\sqrt{\left(y_{\text{off}} - \frac{3ntx_{\text{off}}}{2}\right)^2 + x_{\text{off}}^2} \tag{21a}$$

$$d_i = \frac{1}{2}A_0 \tag{21b}$$

$$\phi_i = \tan^{-1}\left(\frac{x_{\text{off}}}{y_{\text{off}} - \frac{3ntx_{\text{off}}}{2}}\right) \tag{21c}$$

$$\alpha_i = -\alpha \tag{21d}$$

$$B_i = B_0 \tag{21e}$$

$$\beta_i = -\beta \tag{21f}$$

Ignoring the constant offset of $3d_i$ as well as the phase angles ϕ_i and α_i, the equations for X_p and Y_p are equivalent to the parametric equations of an *epitrochoid*. An epitrochoid is the curve traced by a point attached to a circle rolling around the outside of a fixed circle without slip*. In the case of Eq. (20), the radius of both circles is equal to r_i, and the distance between the generating point and the center of the rolling circle is equal to d_i (arm length). The fixed circle is offset by $3d_i$ away from the frame origin (the chief). The phase angle α_i rotates the epitrochoid curve around the $\hat{\boldsymbol{p}}_3$ axis, and ϕ_i is a phase offset of the rolling circle. The phase offset ϕ_i is zero unless $x_{\text{off}} \neq 0$. Drift motion through an orbit-radial offset x_{off} changes the radius r_i of the circles and the phase offset ϕ_i over time. That is, only r_i and ϕ_i are time-varying if the orbit-radial offset x_{off} is non-zero. The Z_p motion still corresponds to a simple unforced oscillator with amplitude B_i and phase angle β_i.

Similar to the elliptic relative orbit shape in the Hill frame, the epitrochoid-based formulation provides an intuitive description of the relative motion in the perifocal frame and consequently the inertial frame, as shown in Fig. 4. The six inertial frame relative orbit elements (IROEs) in Eq. (21) are the invariants of the inertial frame relative motion:

- Circle radius r_i
- Arm length d_i
- Phase offset of rolling circle ϕ_i
- In-plane rotation α_i
- Out-of-plane sinusoidal amplitude B_i
- Out-of-plane phase angle β_i

Closed Relative Orbits

For a closed relative orbit (no drift motion), the orbit-radial offset in the CW equations must be zero, i.e. $x_{\text{off}} = 0$. The shape and size of the inertial frame relative orbit are determined by r_i and d_i. Figure 5 shows inertial frame relative orbits for several different values of r_i and d_i, with all

*see https://en.wikipedia.org/wiki/Epitrochoid. The equations only differ by a phase offset $\theta = \pi/2 - nt$ and are mirrored with $x = -X_p$. Last accessed December 16, 2024.

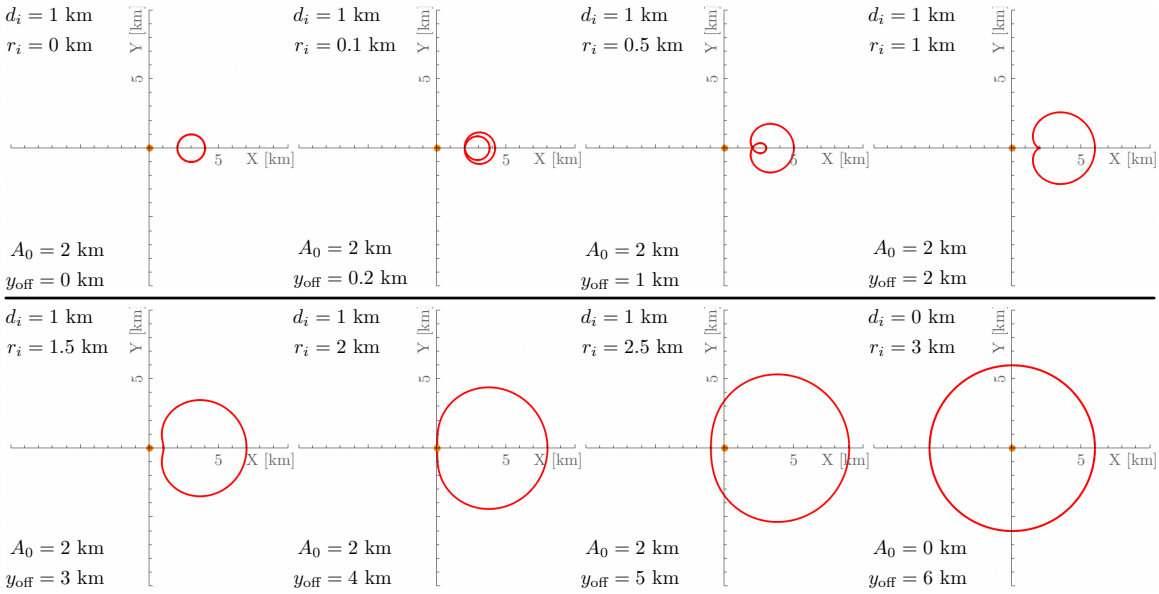

Figure 5: Inertial frame relative orbits for circular chief orbits: The size of the relative orbit changes with r_i, while the shape changes with the ratio of r_i and d_i.

remaining IROEs equal to zero. If $r_i = 0$, the relative orbit shape is circular. The target completes to revolutions of this circle during one orbital period. This is more clear when r_i is slightly increased from 0 to 0.2, where an inner loop becomes visible. Increasing r_i causes the relative orbit size to grow, while the inner loop becomes smaller. The inner loop disappears when $r_i = d_i$. Increasing r_i even more makes the the relative orbit shape more circular. If $d_i = 0$, the relative orbit is circular and centered at the chief, with one revolution per orbital period.

As mentioned in the discussion about the inertial frame relative motion invariants, the relative orbit is offset from the chief by a distance of $3d_i$. Increasing r_i increases the relative orbit size due to the greater size of the circles that generate the epitrochoid curve. The ratio of r_i and d_i determines the shape of the relative orbit. If $r_i < d_i$, the the generating point is outside the rolling circle, creating an inner loop. If $r_i = d_i$, the generating point is on the surface of the rolling circle, creating a cusp. Finally, if $r_i > d_i$, the generating point is inside the rolling circle, creating a curve that becomes circular as $d_i \to 0$.

Drift Motion

An orbit-radial offset x_{off} causes drift of the deputy with respect to the chief due to the difference in semi-major axis of the two spacecraft and that results in different orbital periods. In the Hill frame, the drift motion occurs in the x-direction. In the inertial frame, the drift motion results in a change of the circle radius r_i and the in-plane phase offset ϕ_i over time. Such inertial frame drift motion is shown in Fig. 6. Because r_i changes while d_i remains constant, the shape (inner loop, cusp, no loop) of the epitrochoid changes over time as well.

General Chief Orbit Orientation

In Eq. (20), the relative motion is described in the perifocal frame, which corresponds to the inertial frame only if $\Omega = i = \omega = 0$. However, the derived inertial relative orbit elements are

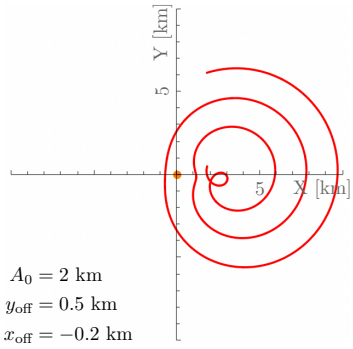

Figure 6: Drift motion in the inertial frame: An offset x_{off} causes the radius r_i to change over time.

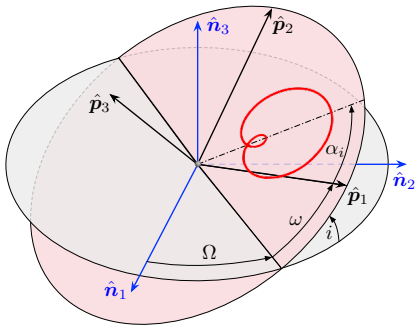

Figure 7: Effect of chief orbit orientation (Ω, i, ω) on inertial frame relative motion: the relative motion may be conveniently described in the perifocal frame, as the mapping from perifocal frame to inertial frame is a pure rotation.

considered to be the relevant parameters for the inertial frame relative motion, because for general chief orbit elements only the orientation of the relative orbit changes, but not the shape. Unlike the transition from the Hill frame $\mathcal{H}$ to the perifocal frame $\mathcal{P}$, which results in a general change of the relative orbit shape, the mapping from the perifocal frame $\mathcal{P}$ to the inertial frame $\mathcal{N}$ is straightforward as it is a pure rotation. The effect of the chief orbit orientation due to (Ω, i, ω) on the orientation of the inertial frame relative orbit is illustrated in Fig. 7.

ELLIPTIC CHIEF ORBITS

The Clohessy-Wilsthire equations assume a circular chief orbit and are not applicable to general chief orbit eccentricities. For elliptic chief orbits, the orbit element difference description is more appropriate. Using Eqs. (14) and (17) results after several simplification steps in the analytical

expression

$$\begin{bmatrix} X_p(f) \\ Y_p(f) \\ Z_p(f) \end{bmatrix} = \begin{bmatrix} r\left(\frac{\delta a \cos f}{a} - \frac{\delta e(2e\cos f - \cos(2f)+3)}{2\eta^2} - \frac{\delta M(\sin f + e\sin f\cos f)}{\eta^3} - \delta\omega\sin f - \delta\Omega\cos i\sin f\right) \\ r\left(\frac{\delta a \sin f}{a} + \frac{\delta e\sin(2f)}{2\eta^2} + \delta M\frac{2(1+e^2)\cos f + e\cos(2f)+3e}{2\eta^3} + \delta\omega\cos f + \delta\Omega\cos i\cos f\right) \\ r\left(\delta i\sin\theta - \delta\Omega\sin i\cos\theta\right) \end{bmatrix} \tag{22}$$

Similar to the inertial frame transformation for circular chief orbits, Eq. (19) is used to rewrite and simplify Eq. (22):

$$\begin{bmatrix} X_p(f) \\ Y_p(f) \\ Z_p(f) \end{bmatrix} = \begin{bmatrix} \frac{\eta^2}{1+e\cos f}\left((3+2e\cos f)d_i\cos\alpha_i - d_i\cos(2f-\alpha_i) - 2r_i\sin(f-\phi_i)\right) \\ \frac{\eta^2}{1+e\cos f}\left((3+2e\cos f)d_i\sin\alpha_i - d_i\sin(2f-\alpha_i) + 2r_i\cos(f-\phi_i)\right) \\ \frac{\eta^2}{1+e\cos f}B_i\cos(\omega+f-\beta_i) \end{bmatrix} \tag{23}$$

Aside from the $2e\cos f$ term and the formulation as function of true anomaly f instead of time t, the form of these equations is the same as in Eq. (20). All components are multiplied by the chief orbit radius r, which is a function of f. For elliptic chief orbits and the differential orbit elements description, the inertial frame relative orbit elements are determined by

$$r_i = \frac{a}{2}\sqrt{\left(\frac{1}{\eta^3}\delta M + \cos i\delta\Omega + \delta\omega\right)^2 + \left(\frac{\delta a}{a}\right)^2} \tag{24a}$$

$$d_i = \frac{a}{2\eta^3}\sqrt{(\eta\delta e)^2 + (e\delta M)^2} \tag{24b}$$

$$\phi_i = \tan^{-1}\left(\frac{\frac{\delta a}{a}}{\frac{1}{\eta^3}\delta M + \cos i\delta\Omega + \delta\omega}\right) \tag{24c}$$

$$\alpha_i = \tan^{-1}\left(\frac{e\delta M}{-\eta\delta e}\right) \tag{24d}$$

$$B_i = a\sqrt{\delta i^2 + (\sin i\delta\Omega)^2} \tag{24e}$$

$$\beta_i = \tan^{-1}\left(\frac{\delta i}{-\sin i\delta\Omega}\right) \tag{24f}$$

Note that several of these IROEs are a function of the same differential orbital elements. However, if one wants to specify d_i and α_i, for example, and determine the values for δe and δM that result in these specified parameters, it is rather straightforward to substitute one equation into the other and solve for δe and δM. For $e = 0$, this differential orbit element description may be used for the circular chief orbit relative motion. However, if $e = 0$, the in-plane rotation α_i can not be adjusted through δe and δM. Instead, a true anomaly phase shift $f = nt - f_0$ must be used.

Figure 8 shows various closed inertial frame relative orbits for an elliptic chief orbit with eccentricity of $e = 0.5$ and semi-major axis of $a = 10000$ km. For the DOE description, δe is similar to the in-plane amplitude A_0 for the circular chief orbit, while $\delta\omega$ is similar to the along-track offset y_{off}. An eccentric orbit essentially stretches part of the 2-by-1 relative orbit ellipse in the Hill frame in the y-direction. This is due to the dependence of the relative motion on the chief orbit radius r, which is the greatest at apoapsis. The part of the Hill frame relative orbit ellipse that is stretched the most in the y-direction corresponds to the part that is traversed while the spacecraft are on the apoapsis side of the orbit. This is visible for the inertial frame relative orbits in Fig. 8 as well. For

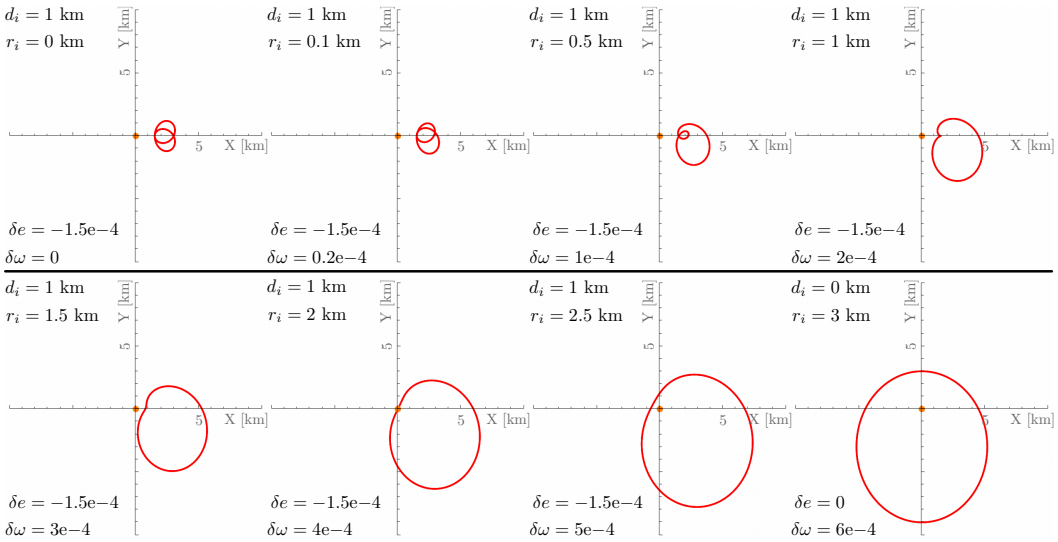

Figure 8: Inertial frame relative orbits for elliptic chief orbits: The relative orbit is stretched for elliptic chief orbits.

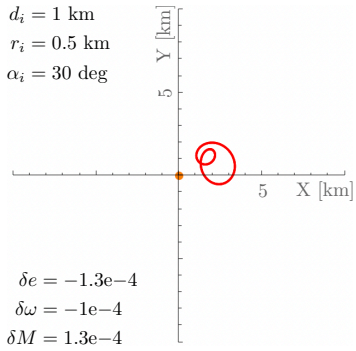

Figure 9: Rotation of inertial frame relative orbit for elliptic chief orbits: a rotation by α_i also changes the relative orbit shape.

$\delta e = -1.5\text{e}-4$, the inertial frame relative orbit is stretched equally in the $-Y_p$ and $+Y_p$ direction. For a positive $\delta\omega$ the relative orbit stretches more in the $-Y_p$ direction. This is because $\delta\omega$ offset shifts the relative orbit in the $+y$ direction of the Hill frame and stretches the orbit more in the $+y$ direction than the $-y$ direction. This stretched part of the relative orbit is traversed when the $+y$ direction of the Hill frame is pointing in the $-Y_p$ direction of the perifocal frame, resulting in a larger relative orbit part in $-Y_p$ Similar to the circular chief orbit case, increasing r_i while d_i remains the same causes the inner loop to disappear and turn into a cusp when $r_i = d_i$. Increasing r_i further such that $r_i > d_i$ makes the inertial frame relative orbit more and more elliptic. If $d_i = 0$, the relative orbit is elliptic in the inertial frame.

An example for the inertial frame orbit rotation for an elliptic chief orbit is shown in Fig. 9. To induce a rotation of α_i, the ratio of $(e\delta M)/(-\eta\delta e)$ must be changed. To maintain the same d_i, $e\delta M$ and $-\eta\delta e$ cannot be arbitrarily changed, however, and $\delta\omega$ must be adjusted as well such that r_i remains the same. Thus, the relative orbit shape changes when a rotation of α_i is applied.

The effect of the chief orbit orientation (Ω, i, ω) on the relative orbit shape in the perifocal frame is already considered in Eq. (23). The remaining rotation of the relative orbit through (Ω, i, ω) is the same for the elliptic orbit as for the circular orbit, as illustrated in Fig. 7.

CONCLUSIONS

This paper investigates the relative motion of two spacecraft as seen from a frame that is centered at the chief spacecraft and with axes that are aligned with an inertial frame. Such an inertial frame description is beneficial compared to the conventional rotating Hill frame when the relative motion is subject to inertially fixed constraints. Examples for such missions include inertial targets for distributed space telescopes and coronagraphs, spacecraft formations and servicing operations with constraints imposed by the Sun (lighting conditions, eclipses, space plasma conditions, etc.), as well as rendezvous with a non-rotating target. The last example is relevant because the body frame of a non-rotating body remains aligned with the inertial frame, and body frames are frequently used for servicing and docking operations.

It is found that the inertial frame relative motion for a circular chief orbit is equivalent to the epitrochoid curve, in which a circle rolls without slip on a fixed circle, and the curve is generated by a point that is at a certain distance away from the center of the rolling circle. Thus, inertial frame relative orbit elements (IROEs) are defined that are based on the parameters of an epitrochoid curve and correspond to the invariants of relative motion in the inertial frame. This allows for an intuitive description of the inertial frame relative motion. For elliptic chief orbits, the inertial frame relative orbits are stretched and distorted compared to the epitrochoid curve for circular chief orbits, but similar IROEs are defined as well.

ACKNOWLEDGMENTS

Julian Hammerl gratefully acknowledges funding from the NASA FINESST fellowship (award number 80NSSC22K1849) and the Dr. George H. Born Endowed Fund Travel Award.

REFERENCES

[1] G. W. Hill, "Researches in the Lunar Theory," *American Journal of Mathematics*, Vol. 1, No. 1, 1878, pp. 5–26, 10.2307/2369430.

[2] W. H. Clohessy and R. S. Wiltshire, "Terminal Guidance System for Satellite Rendezvous," *Journal of the Aerospace Sciences*, Vol. 27, No. 9, 1960, pp. 653–658, 10.2514/8.8704.

[3] A. W. Koenig, S. D'Amico, B. Macintosh, and C. J. Titus, "Optimal Formation Design of a Miniaturized Distributed Occulter/Telescope in Earth Orbit," *2015 AAS/AIAA Astrodynamics Specialist Conference*, 2015, pp. 1–29.

[4] J. Kolmas, P. Banazadeh, A. W. Koenig, B. Macintosh, and S. D'Amico, "System design of a miniaturized distributed occulter/telescope for direct imaging of star vicinity," *2016 IEEE Aerospace Conference*, 2016, pp. 1–11, 10.1109/AERO.2016.7500783.

[5] A. Koenig, S. D'Amico, and E. G. Lightsey, "Formation flying orbit and control concept for the VISORS mission," *AIAA Scitech 2021 Forum*, 2021, pp. 1–22.

[6] W. Cash, S. Kendrick, C. Noecker, J. Bally, J. DeMarines, J. Green, P. Oakley, A. Shipley, S. Benson, S. Oleson, D. Content, D. Folta, S. Garrison, K. Gendreau, K. Hartman, J. Howard, T. Hyde, D. Lakins, J. Leitner, D. Leviton, R. Luquette, B. Oegerley, K. Richon, A. Roberge, S. Tompkins, J. Tveekrem, B. Woodgate, M. Turnbull, D. Dailey, K. Decker, R. Dehmohseni, B. Gaugh, T. Glassman, M. Haney, R. Hejal, C. Lillie, A. Lo, D. O'Conner, G. Oleas, R. Polidan, R. Samuele, S. Shields, J. Shirvanian, D. SooHoo, G. Tinetti, B. Dorland, R. Dudik, R. Gaume, and B. Mason, "The New Worlds Observer: the astrophysics strategic mission concept study," *UV/Optical/IR Space Telescopes: Innovative Technologies and Concepts IV* (H. A. MacEwen and J. B. Breckinridge, eds.), Vol. 7436, International Society for Optics and Photonics, SPIE, 2009, p. 743606, 10.1117/12.827486.

[7] T. Glassman, A. S. Lo, J. Arenberg, W. Cash, and C. Noecker, "Starshade scaling relations," *Techniques and Instrumentation for Detection of Exoplanets IV* (S. B. Shaklan, ed.), Vol. 7440, International Society for Optics and Photonics, SPIE, 2009, p. 744013, 10.1117/12.825033.

[8] M. Aung, A. Ahmed, M. Wette, D. Scharf, J. Tien, G. Purcell, M. Regehr, and B. Landin, "An overview of formation flying technology development for the Terrestrial Planet Finder mission," *2004 IEEE Aerospace Conference Proceedings (IEEE Cat. No.04TH8720)*, Vol. 4, 2004, pp. 2667–2679 Vol.4, 10.1109/AERO.2004.1368062.

[9] A. M. Glauser, S. P. Quanz, J. Hansen, F. Dannert, M. Ireland, H. Linz, O. Absil, E. Alei, D. Angerhausen, T. Birbacher, D. Defrère, A. Fortier, P. A. Huber, J. Kammerer, R. Laugier, T. Lichtenberg, L. Noack, M. Ranganathan, S. Rugheimer, V. Airapetian, Y. Alibert, P. J. Amado, M. Anger, N. Anugu, M. Aragon, D. J. Armstrong, A. Balbi, O. Balsalobre-Ruza, D. Banik, M. Beck, S. Bhattarai, J. Biren, J. Bottoni, M. Braam, A. Brandeker, L. A. Buchhave, J. A. Caballero, J. Cabrera, L. Carone, Ó. Carrión-González, A. Castro-González, K. Chan, L. F. Coelho, T. Constantinou, N. Cowan, W. Danchi, C. Dandumont, J. Davoult, A. Dawn, J.-P. P. d. Vera, P. J. d. Visser, C. Dorn, J. A. D. Lara, M. Elowitz, S. Ertel, Y. Fang, S. Felix, J. Fortney, M. Fridlund, A. G. Muñoz, C. Gillmann, G. Golabek, J. L. Grenfell, G. Guidi, O. Guilera, J. Hagelberg, J. Hansen, J. Haqq-Misra, N. Hara, R. Helled, K. Herbst, N. Hernitschek, S. Hinkley, T. Ito, S. Itoh, S. Ivanovski, M. Janson, A. Johansen, H. Jones, S. Kane, D. Kitzmann, A. B. Kovacevic, S. Kraus, O. Krause, J. M. D. Kruijssen, R. Kuiper, A. Kuriakose, L. Labadie, S. Lacour, A. F. Lanza, L. Leedjärv, M. Lendl, M. Leung, J. Lillo-Box, J. Loicq, R. Luque, S. Mahadevan, L. Majumdar, F. Malbet, F. Mallia, J. Mathew, T. Matsuo, E. Matthews, V. Meadows, B. Mennesson, M. R. Meyer, K. Molaverdikhani, P. Mollière, J. Monnier, R. Navarro, B. Nsamba, K. Oguri, A. Oza, E. Palle, C. Persson, J. Pitman, E. Plávalová, F. J. Pozuelos, A. Quirrenbach, R. Ramirez, A. Reiners, I. Ribas, M. Rice, B. V. Ricketti, P. Roelfsema, A. Romagnolo, M. P. Ronco, M. Schlecker, J. Schonhut-Stasik, E. Schwieterman, A. A. Sefilian, E. Serabyn, C. Shahi, S. Sharma, L. Silva, S. Singh, E. L. Sneed, L. Spencer, V. Squicciarini, J. Staguhn, K. Stapelfeldt, K. Stassun, M. Tamura, B. Taysum, F. v. d. Tak, T. A. v. Kempen, G. Vasisht, H. S. Wang, R. Wordsworth, and M. Wyatt, "The Large Interferometer For Exoplanets (LIFE): a space mission for mid-infrared nulling interferometry," *Optical and Infrared Interferometry and Imaging IX* (J. Kammerer, S. Sallum, and J. Sanchez-Bermudez, eds.), Vol. 13095, International Society for Optics and Photonics, SPIE, 2024, p. 130951D, 10.1117/12.3019090.

[10] D. Scheeres and N. Vinh, "Dynamics and control of relative motion in an unstable orbit," *Astrodynamics Specialist Conference*, 2000, p. 4135.

[11] L. Bucci, A. Colagrossi, and M. Lavagna, "Rendezvous in lunar near rectilinear halo orbits," *Advances in Astronautics Science and Technology*, Vol. 1, 2018, pp. 39–43.

[12] J. Wang and D. Hastings, "Ionospheric plasma flow over large high-voltage space platforms. II: The formation and structure of plasma wake," *Physics of Fluids B: Plasma Physics*, Vol. 4, No. 6, 1992, pp. 1615–1629.

[13] C. R. Seubert, L. A. Stiles, and H. Schaub, "Effective Coulomb force modeling for spacecraft in Earth orbit plasmas," *Advances in Space Research*, Vol. 54, No. 2, 2014, pp. 209–220, 10.1016/j.asr.2014.04.005.

[14] K. Wilson and H. Schaub, "Impact of Electrostatic Perturbations on Proximity Operations in High Earth Orbits," *Journal of Spacecraft and Rockets*, Vol. 58, No. 5, 2021, pp. 1293–1302, 10.2514/1.A35039.

[15] D. E. Hastings, "A review of plasma interactions with spacecraft in low Earth orbit," *Journal of Geophysical Research: Space Physics*, Vol. 100, No. A8, 1995, pp. 14457–14483, https://doi.org/10.1029/94JA03358.

[16] R. E. Ergun, D. M. Malaspina, S. D. Bale, J. P. McFadden, D. E. Larson, F. S. Mozer, N. Meyer-Vernet, M. Maksimovic, P. J. Kellogg, and J. R. Wygant, "Spacecraft charging and ion wake formation in the near-Sun environment," *Physics of Plasmas*, Vol. 17, 07 2010, p. 072903, 10.1063/1.3457484.

[17] J. Sullivan, S. Grimberg, and S. D'Amico, "Comprehensive Survey and Assessment of Spacecraft Relative Motion Dynamics Models," *Journal of Guidance, Control, and Dynamics*, Vol. 40, No. 8, 2017, pp. 1837–1859, 10.2514/1.G002309.

[18] A. B. Roger and C. R. McInnes, "Safety Constrained Free-Flyer Path Planning at the International Space Station," *Journal of Guidance, Control, and Dynamics*, Vol. 23, No. 6, 2000, pp. 971–979, 10.2514/2.4656.

[19] H. Dong, Q. Hu, and M. R. Akella, "Safety Control for Spacecraft Autonomous Rendezvous and Docking Under Motion Constraints," *Journal of Guidance, Control, and Dynamics*, Vol. 40, No. 7, 2017, pp. 1680–1692, 10.2514/1.G002322.

[20] S. W. Albert and H. Schaub, "Relative Motion in the Velocity Frame for Atmospheric Entry Trajectories," *Journal of Spacecraft and Rockets*, Vol. 60, No. 5, 2023, pp. 1614–1624, 10.2514/1.A35753.

[21] B. Naasz, "Safety ellipse motion with coarse sun angle optimization," *595 Flight Mechanics Symposium*, 2005.

[22] Y. Yao, R. Xie, and F. He, "Flyaround Orbit Design for Autonomous Rendezvous Based on Relative Orbit Elements," *Journal of Guidance, Control, and Dynamics*, Vol. 33, No. 5, 2010, pp. 1687–1692, 10.2514/1.48494.

[23] H. Schaub and J. L. Junkins, *Analytical Mechanics of Space Systems*. Reston, VA: AIAA Education Series, 4th ed., 2018, 10.2514/4.105210.